Microporous and Mesoporous Materials 154 (2012) 100–106

Contents lists available at SciVerse ScienceDirect

Microporous and Mesoporous Materials

journal homepage: www.elsevier.com/locate/micromeso

Influence of the textural properties of Rh/MOF-5 on the catalytic properties in the hydroformylation of olefins

Toan Van Vu [a,b], Hendrik Kosslick [a,b,*], Axel Schulz [a,b,*], Jörg Harloff [a], Eckhard Paetzold [b], Henrik Lund [a], Udo Kragl [a,b], Matthias Schneider [b], Gerhard Fulda [c]

[a] Institute for Chemistry, University of Rostock, Albert Einstein Str. 3a, D-18059 Rostock, Germany
[b] Leibniz-Institute for Catalysis at the University of Rostock, Albert Einstein Str. 29a, D-18059 Rostock, Germany
[c] Center for Electronmicroscopy, Institute of Pathology, University of Rostock, Strempel Str. 14, D-18057 Rostock, Germany

ARTICLE INFO

Article history:
Available online 13 December 2011

Keywords:
Heterogeneous catalysis
Olefins
Hydroformylation
Metal–organic framework
Texture

ABSTRACT

Rh/MOF-5 catalysts have been prepared and characterized by XRD, FTIR, nitrogen adsorption, and TEM. MOFs with different textural properties, namely nano-sized materials and larger crystals, were obtained by changing synthesis conditions. The catalytic properties of the different samples were tested in the hydroformylation reaction of olefins. It is shown that the catalytic properties of nano-sized Rh/MOF-5 catalysts markedly differ from that of larger crystals. Especially, the selectivity to *n*-aldehydes is clearly improved. However, also the double bond isomerization side reaction is enhanced. The results confirm the potential of MOFs for the application as catalyst supports.

1. Introduction

The discovery of metal–organic frameworks (MOFs) has opened a variety of new opportunities for potential applications of these materials in catalysis, separation, and other uses [1–7]. This material possesses extra-ordinary of properties such as very high specific surface areas, tunable and extra large pore sizes, the organic–inorganic hybrid character with strictly alternating arrangement of hydrophobic linker and hydrophilic metal oxide sites, and the vast possibilities to functionalize, modify, or exchange organic linkers and metal compartments, which make MOFs special compared to common micro and mesoporous materials [8–13]. Therefore, MOFs are very interesting materials for the application in heterogeneous catalysts or catalyst supports [14,15].

The hydroformylation reaction is one of the most important homogeneous catalyzed reactions in chemical industry [16–18]. It was discovered by Otto Roelen in 1938 [19,20]. The reaction of olefinic double bonds with synthesis gas yields linear and branched aldehydes as primary products [21].

Linear aldehydes, which are needed in larger amounts than branched aldehydes, can be used for the production of alcohols. Approximate 9 million metric tons/year of aldehydes and alcohols are produced using the hydroformylation reaction [22]. These products are starting materials for the synthesis of plasticizers, detergents, adhesives, solvents as well as pharmaceuticals and agrochemicals [23,24].

Both cobalt and rhodium complexes can be used as homogeneous catalysts in the industrial process for hydroformylation. Improvements of rates and selectivities by ligand design as well as mechanistic aspects have much received attention to optimize the homogeneous process [18]. However, there are some limits in the homogeneous hydroformylation process. One of these disadvantages is the separation of the catalyst from product mixture [16,22,25]. Therefore, heterogenization of rhodium complex for hydroformylation has been received great efforts.

Numerous support materials for rhodium complex have been reported for this reaction. The materials studied include MCM-41, silica, alumina, zeolites, activated carbons, polymeric organic, inorganic, and hybrid supports, or supported aqueous phase catalyst (SAPC) [21,26–31]. Main disadvantages of these supported catalysts are leaching of rhodium complex during the reaction, complicated synthesis procedure, lower catalyst activity, selectivity, and thermal instability [22].

Encouraged by the outstanding properties, in this study, we further evaluate the potential of MOFs for the application as catalyst support in the hydroformylation reaction. In detail, the catalytic properties and the influence of textural properties of Rh/MOF-5, as particle size, are studied. The catalytic conversion of several types of olefins such as linear/branched olefins, and cycloolefins has been investigated. Additionally, olefin mixture is also employed. It will be

* Corresponding authors. Address: Institute for Chemistry, University of Rostock, Albert Einstein Str. 3a, D-18059 Rostock, Germany. Tel.: +49 381 498 6384; fax: +49 381 498 6382.
E-mail addresses: hendrik.kosslick@uni-rostock.de (H. Kosslick), axsl.schulz@uni-rostock.de (A. Schulz).

1387-1811/$ - see front matter © 2011 Elsevier Inc. All rights reserved.
doi:10.1016/j.micromeso.2011.11.052

shown that the textural properties have an important impact on the catalytic properties, especially, on the selectivity to *n*-aldehydes, and the double bond isomerization reaction.

2. Experiment

2.1. Preparation

2.1.1. Synthesis of MOF-5

MOF-5 was synthesized by optimized procedures based on literature [32–36]. As starting materials $Zn(NO_3)_2$ (zinc nitrate), H_2BDC (terephthalic acid), and the solvent DMF (dimethylformamide) were used. The solvent was distilled and dried over calcium hydride before use. The sample of MOF-5 (A) was synthesized as follows.

3.32 g of H_2BDC (Merck) and 15.69 g of $Zn(NO_3)_2 \cdot 4H_2O$ (Merck) were dissolved into 500 ml of DMF (Merck). The solution was given into a glass reactor which was equipped with a drying tube on overhead end. The mixture was heated to 105 °C under stirring. Then the mixture was allowed to crystallize by standing at 105 °C for 24 h under static condition. Thereafter, the reaction mixture was allowed to cool down to room temperature.

The crystallized product was filtered off and washed three times with 3×10 ml of CH_2Cl_2. The recovered solid was suspended in 50 ml of DMF, heated under stirring to 130 °C, and held at this temperature for 1 h. Then the solid was filtered off and washed 3 times with 3×10 ml of CH_2Cl_2. Next, it was given into 50 ml of CH_2Cl_2 and stirred for 12 h at room temperature. Thereafter, the solid was again filtered off and washed three times with 3×10 ml of CH_2Cl_2. The repeated work up was conducted to remove residual H_2BDC and low volatile DMF solvent in the synthesized product. Finally, the fine powder product, considered as MOF-5 (A), was achieved by drying the solid under vacuum condition at 105 °C for 12 h. Further two samples of different texture, nano-sized MOF-5 (B) and large crystal MOF-5 (C), were obtained by changing synthesis conditions as aging of the reaction for some hours before solvothermal crystallization under stirring (B) and treatment in autoclave under static condition (non-stirred) at autogeneous pressure (C) with the same composed synthesis mixture.

2.1.2. Rhodium loading

A solution containing 28 ml of acetonitrile (Baker), 10 mg of Rh(acac) (cod) [(acetylacetonato)(cycloocta-1,5-diene)rhodium(I)], and 20 ml of toluene (Merck) was added to 4 g of MOF-5(A) in a glass vessel. The mixture was heated and continuously stirred at 70 °C in order to evaporate the solvent and to adsorb the rhodium precursor on the support (evaporation–deposition). The material was dry after 2.5 h. Then the powder was washed three times with 3×5 ml of toluene. After washing, the solid was dried in the oven at 70 °C for 24 h. This material was used as starting Rh/MOF-5 (A) supported catalyst with a rhodium concentration of 0.1 wt.%. Sample (B) and (C) were supported with rhodium in the same way.

2.2. Characterization

The structures of samples were checked by XRD. Powder diffraction measurements were carried out on X-ray diffractometer STADI-P (STOE) using Ni-filtered Cu K_α radiation ($\lambda = 1.5418$ Å). IR spectroscopic studies were carried out in ATR (attenuated total reflection) mode using a Nicollet 380 FTIR spectrometer coupled with smart orbit ATR device with a resolution of 4 cm^{-1}.

Textural properties were studied by TEM and nitrogen sorption measurements. Prior to TEM measurements, powdered MOF-5 samples were dispersed in ethanol and deposited on copper grids. Electron microscopy experiments were done on a LIBRA 120 at 120 kV. Images were recorded with a digital camera with 2000×2000 pixels. Nitrogen adsorption measurements were performed on an ASAP 2010 sorption system. Before measurement, the solvent in the samples was removed by heating and pumping under reduced pressure at *ca.* 150 °C. Nitrogen adsorption measurements were carried out at 77 K.

2.3. Catalytic testing

Linear olefins with different chain length like *n*-hexene-1 ($\geqslant$97%, Aldrich), *n*-octene-1 ($\geqslant$98%, Aldrich), *n*-decene-1 ($\geqslant$95%, Acros), and *n*-dodecene-1 (93–95%, Acros) were used for *n*-alkene-1 hydroformylation studies over Rh/MOF-5 catalysts. Some branched olefins as 3,3-dimethyl-1-butene ($\geqslant$95%, Aldrich), 4,4-dimethyl-1-pentene ($\geqslant$99%, SAFC), and 2,4,4-trimethyl-1-pentene ($\geqslant$99%, Sigma–Aldrich) as well as bulky cyclohexene ($\geqslant$99%, Sigma–Aldrich) and cyclooctene ($\geqslant$95%, Acros) were also included in the catalytic testing. Also mixture containing three different olefins was tested in the catalytic experiments.

A 100 ml PARR reactor was filled with the mixture of olefins, toluene (solvent), and the catalyst. After filling, the reactor was evacuated with a vacuum pump. Then the reactor was filled with pressurized argon. Next the argon gas was purged by vacuum pumping. This purging procedure was repeated twice to ensure removal residual air and moisture from the reaction system. After that, the reactor was immediately loaded with synthesis gas up to 50 bars at room temperature (25 °C). Finally, the reaction mixture was heated under stirring and kept at temperature of 100 °C during the course of reaction. The reactor was equipped with gas introduction stirrer operating at a speed of 1000 rpm.

Typically, for *n*-hexene-1 ($C_6^=$) hydroformylation reaction, 95 mg of Rh/MOF-5, 12.5 ml of *n*-hexene-1, and 30 ml of toluene were loaded into the reactor. The *n*-alkene-1/catalyst ratio was maintained at 10.000/1 based on rhodium. The other olefins were hydroformylated in a similar way. The molar olefin/Rh ratios were kept constant at 10.000/1. For reaction with mixture of containing three olefins, the same total olefin/Rh molar ratio was used. Hence, the content of each single olefin was reduced to 67 %.

3. Results and discussion

3.1. Materials

The crystallinity and structure of Rh/MOF-5 catalysts were checked by XRD. They are in agreement with previously reported pattern of MOF-5 [37–39]. The XRD pattern of Rh/MOF-5 (A) material is shown in Fig. 1.

The TEM images of MOF-5 (A) are shown in Fig. 2. They show that MOF-5 (A) consists of well crystallized elongated nanocrystals. The shape is uniform with crystal dimensions of *ca.* 40–50×200 nm. The crystals tend to agglomerate, Fig. 2(a). No indication of additional intraparticle nanoporosity is found in TEM.

For comparison, two other MOF-5 samples of different texture (Table 1) were involved in the study, namely a second nano-sized MOF-5 (B) sample consisting of smaller, less elongated (in size of *ca.* 25×100 nm) and in tendency more intergrown crystals, Fig. 2(b), as well as a well-crystallized MOF-5 (C) material consisting of large crystals up to mm-scale, Fig. 2(c). These crystals contain additional nanopores. Briefly, the synthesis procedure and handling significantly influence the textural property of synthesized metal–organic framework MOF-5.

FTIR spectra of MOF-5 (A) sample and Rh/MOF-5 (A) supported catalyst in the spectral range of 500–2500 cm^{-1} are shown in Fig. 3. They are very well resolved and show the typical vibration bands observed of benzene carboxylate, which is present as a linker.

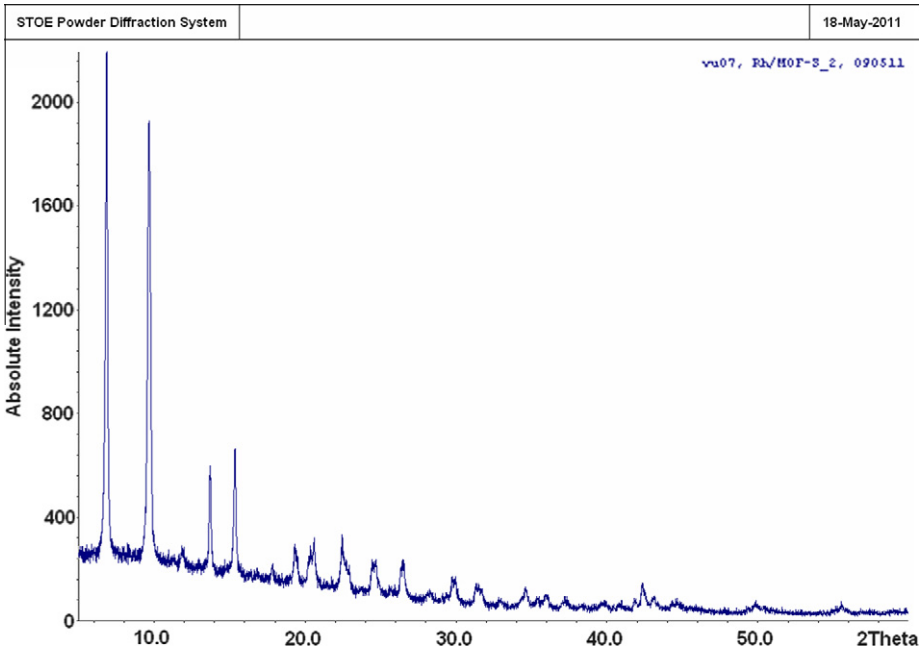

Fig. 1. XRD pattern of Rh/MOF-5 (A).

The spectra are dominated by strong absorbances between about 1350–1600 and 740–825 cm^{-1}. These bands are related to vibration modes of carboxyl groups and different =C–H modes of the phenyl groups. The FTIR lattice vibration spectra shows no indication for partial hydrolysis of the MOF usually indicated by a high frequency shift of the carboxyl vibration band at 1610 cm^{-1} to 1690–1760 cm^{-1}.

Interestingly, Rh loading leads to a markedly low frequency shift of this and other vibration bands by 15–10 cm^{-1} and splitting of the 746 cm^{-1} linker vibration band of the benzene even the loading is low. This confirms that the Rh is located in the framework of MOF-5. The rhodium seems to be highly dispersed. No larger metal particles could be detected in the TEM images. Indeed, detailed studies on the supporting of noble metals on MOF-5 materials show that the Me(cod) complex is decomposed and reduced to Me(0) by hydrogenolysis under hydrogen atmosphere. Thereby small metal nanoclusters are formed [40]. It is expected that the same happens in the case of the prepared Rh/MOF-5 catalysts with much lower Rh loading.

The specific surface area and pore volumes of materials were studied by nitrogen adsorption and desorption measurements. The isotherm shown in Fig. 4 belongs to the type I according to IUPAC nomenclature [41]. Strong nitrogen adsorption at very low relative pressure as indicated by the steep of the isotherm is due to adsorption in the micropores of MOF-5. The further slightly increase of the nitrogen uptake up to a relative pressure *ca.* $p/p_0 = 0.5$ is due to adsorption in small mesopores having diameters of 2–5 nm. TEM shows no intraparticle mesoporosity. Therefore, these pores are due to textural porosity between the MOF nanoparticles.

The BET surface area of MOF-5 (A) is 2337 m^2/g, which is markedly higher than that of the nano-sized MOF-5 (B) as well as the well crystallized MOF-5 (C) sample with the specific surface area of *ca.* 1200 m^2/g (Table 1).

3.2. Catalysis

The catalytic performance of supported Rh/MOF-5 catalyst in the hydroformylation of different sized and branched olefins has been investigated. Along with formation of target *n*- and *i*-aldehydes, double bond shift reaction is observed as side reaction catalyzed by acid sites.

3.2.1. Reactions with single olefin components

The total conversions of different linear *n*-alkene-1 as *n*-hexene-1 ($C_6^=$), *n*-decene-1 ($C_{10}^=$), and *n*-dodecene-1 ($C_{12}^=$) to aldehydes and *i*-alkenes over nano-sized Rh/MOF-5 (A) are shown in Fig. 5. The conversions proceed relatively fast with a nearly linear increase of the conversion with time of reaction. The conversions decrease with increasing chain lengths of the olefins as expected. Total conversions of *ca.* 99%, 90%, and 67% to aldehydes and double bond shifted *i*-olefins are achieved after 5 h of reaction with $C_6^=$, $C_{10}^=$, and $C_{12}^=$, respectively (Fig. 5).

The yields of aldehydes in dependence on the reaction time obtained with *n*-alkene-1 over Rh/MOF-5 (A) are shown in Fig. 6. After 5 h of reactions, *ca.* 45%, 27%, and 19% of $C_6^=$, $C_{10}^=$, and $C_{12}^=$ are converted to aldehydes, respectively. The aldehyde to *i*-alkene (double bond shifted) ratio is nearly unchanged up to 5 h of reaction. Thereafter, the yield of aldehydes is further increased on the expense of olefins, especially *i*-alkenes, in the reaction mixture. However, the reaction proceeds slower. The *i*-alkenes are less reactive. Their diffusivity should be decreased compared to linear ones. As a result, also the *n*/*i*-aldehyde ratio is decreased from 2 to 2.9 in the first 5 h to *ca.* 1.1 after 21 h of reaction (Fig. 7).

Different sized olefins, namely cyclohexene, cyclooctene, and different branched olefins as 3,3-dimethyl-1-butene (DMB), 4,4-dimethyl-1-pentene (DMP), and 2,4,4-trimethyl-1-pentene (TMP) were used as test molecules in order to study the molecular sieve effect (size exclusion) of the microporous MOF-5 framework and to check possible contribution of Rh leaching to the catalytic activity.

Indeed, conversion of the large cycloolefins and the bulky TMB are very low in the first hours of reaction revealed by the aldehyde yields vs. reaction time plots shown in Fig. 8. This provides evidence of active Rh species located inside the MOF crystals. The prevention of conversion of cyclohexene might be due to hindered diffusivity of the formed aldehyde, because cyclohexene is known to be small enough to pass the window of the MOF-5 channels [42].

The conversions of DMB and DMP to aldehydes are somewhat higher compared to the aldehyde yields observed with *n*-dode-

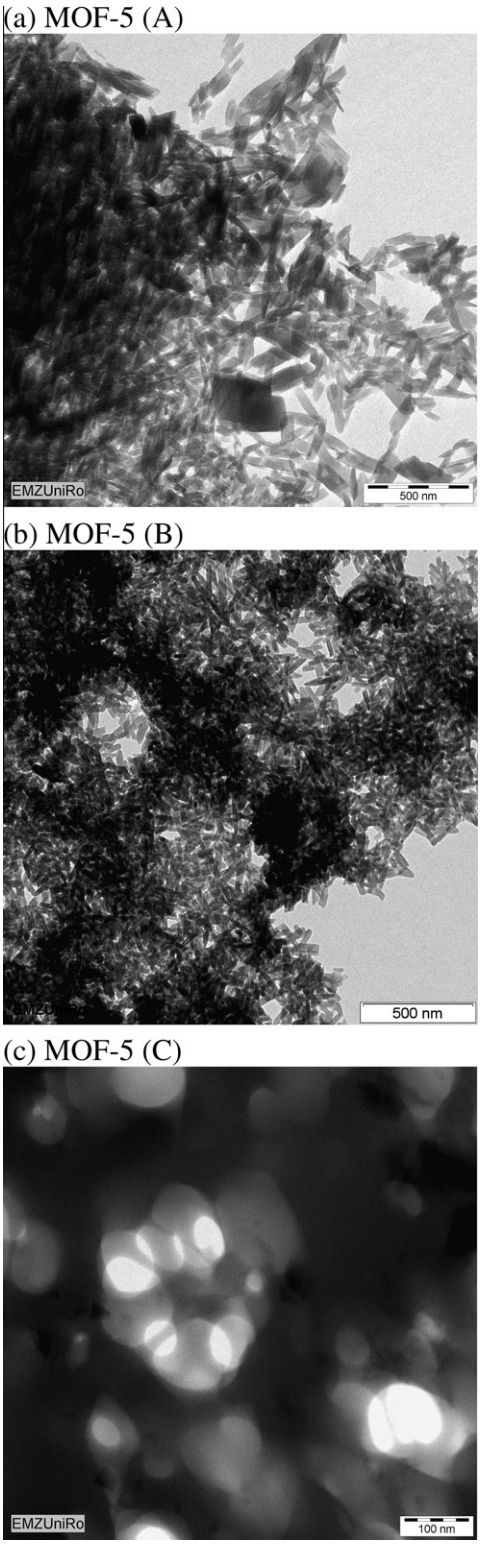

Fig. 2. TEM images of MOF-5 showing nano-sized samples, sample A (a) and sample B (b), as well as TEM image of a microtome cut of the large-sized sample C (c) in bottom. In (c), white areas show nano-sized secondary pores inside the large MOF-5 crystal. (a) MOF-5 (A); (b) MOF-5 (B); (c) MOF-5 (C).

cene-1 (Fig. 6). It seems that the bulky trimethyl head group decreases the access to pores of MOF. But the tail with the C=C group may stick into the outer pores. Therefore, with prolonged reaction time to 21 h a remarkable increase of the aldehyde yield is observed.

Table 1
Specific surface area, specific pore volume and intraparticle porosity of different MOF-5 materials derived from nitrogen adsorption measurements.

Material	BET specific surface area (m^2/g)	Specific pore volume (cm^3/g)	Intraparticle nanoporosity[a] (nm)	Note
MOF-5 (A)	2337	1.0	–	Agglomerated
MOF-5 (B)	576	0.22	25–100	Intergrown
MOF-5 (C)	1200	1.0	–	Microcrystalline

[a] Estimated from TEM images.

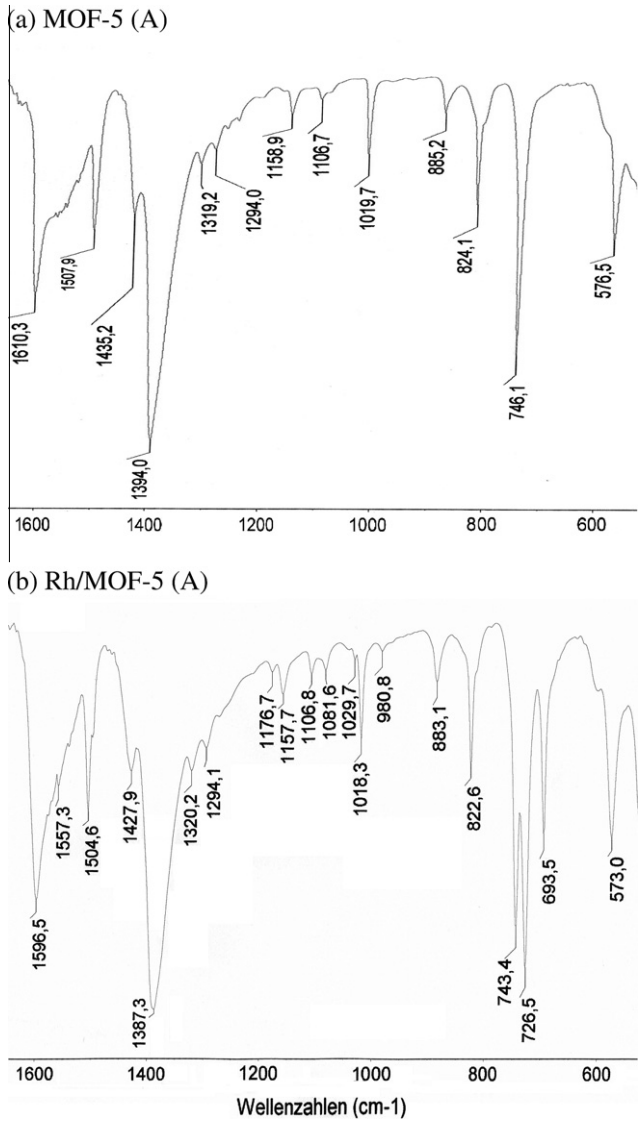

Fig. 3. FTIR spectra of nano-sized (a) MOF-5 support (A) and (b) Rh/MOF-5 supported catalyst (A). (a) MOF-5 (A); (b) Rh/MOF-5 (A).

3.2.2. Reaction with mixtures of olefins

The behavior of olefin mixture in the hydroformylation was tested using mixture of *n*-hexene-1, *n*-octene-1, and cyclohexene. The molar olefin/Rh ratio and the solvent content were the same as for single component experiments (10.000/1). Hence, the concentration of single olefin was lower by 67% compared to the single component run.

The hydroformylation behavior of $C_6^=$, $C_8^=$, and cyclohexene in their mixture are shown in Figs. 9–11. Interestingly, the conversion

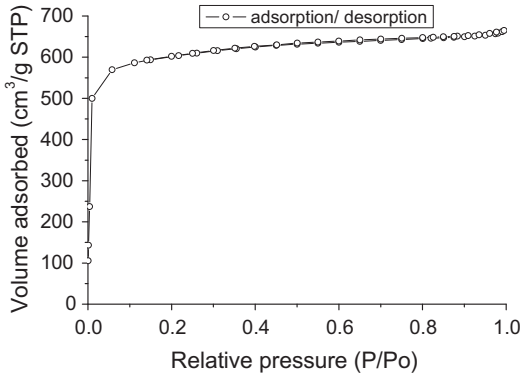

Fig. 4. Nitrogen adsorption and desorption isotherms of MOF-5 (A) measured at 77 K.

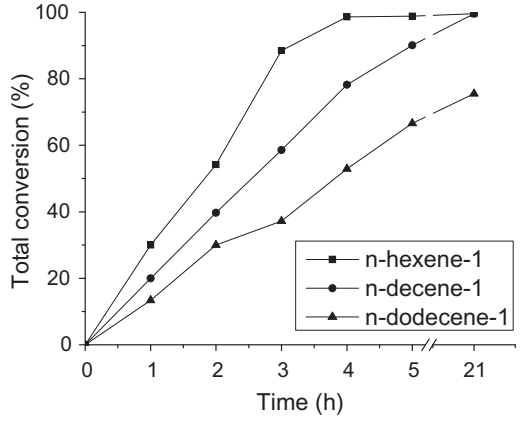

Fig. 5. Total conversion of olefins in hydroformylation catalyzed by Rh/MOF-5 (A) at T = 100 °C, P = 50 bars.

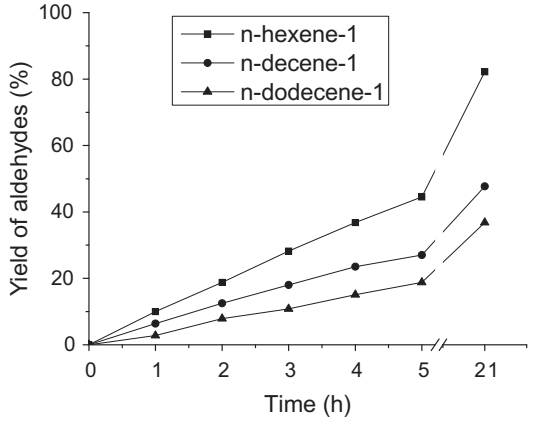

Fig. 6. Yield of aldehydes in hydroformylation of olefins catalyzed by Rh/MOF-5 (A) at T = 100 °C, P = 50 bars.

of $C_6^=$ and $C_8^=$ are similar. This holds also for the aldehyde yields in dependence of reaction time. The total conversion increases over 95% after 5 h of reaction. The yields of aldehydes develop parallel with time and reach *ca.* 32%. As observed with single components, aldehyde yields further increase with prolonged reaction on the expenses of olefins in the mixture. Cyclohexene is nearly excluded from reaction with 1.3 % of conversion after 3 h. This is somewhat lower than observed with the single component (2.8%). The *n*/*i*-aldehyde selectivities obtained with the olefin mixtures are still high with values of *ca.* 2.8 after 5 h of reaction as found with single

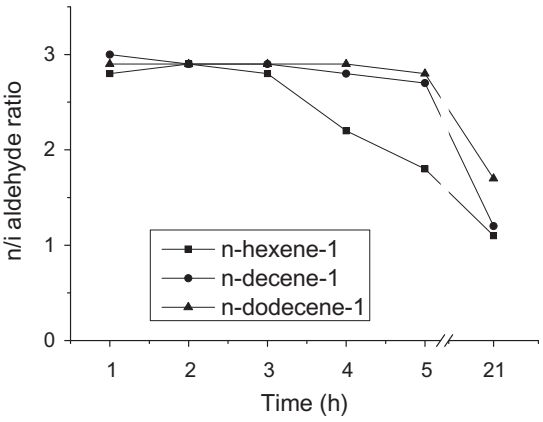

Fig. 7. *n*/*i*-aldehyde ratio in hydroformylation of olefins catalyzed by Rh/MOF-5 (A) at T = 100 °C, P = 50 bars.

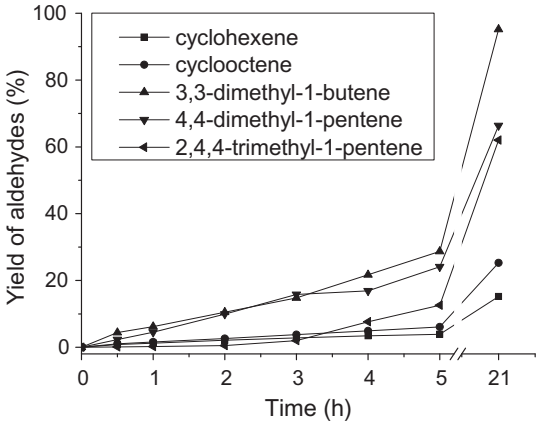

Fig. 8. Yield of aldehydes in hydroformylation of cyclo/branched olefins catalyzed by Rh/MOF-5 (A) at T = 100 °C, P = 50 bars.

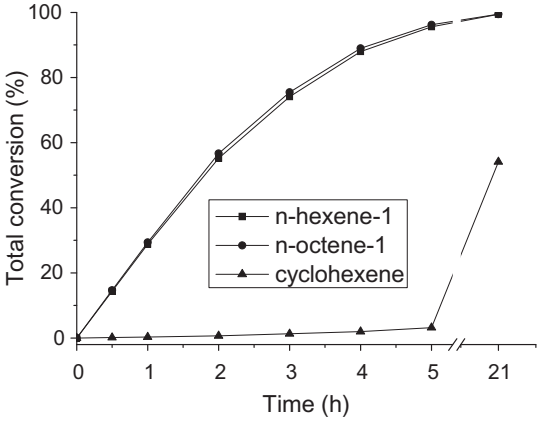

Fig. 9. Total conversion of the mixture of *n*-hexene-1, *n*-octene-1, and cyclohexene in hydroformylation catalyzed by Rh/MOF-5 (A) at T = 100 °C, P = 50 bars.

components (7). With prolonged reaction, this ratio is distinctly decreased to 1.3 and 0.94 for $C_6^=$ and $C_8^=$, respectively, due to the conversion of *i*-olefins (Fig. 11).

3.2.3. Influence of texture on catalytic behavior

The influence of the texture was studied using three different MOF-5 samples obtained from synthesis mixtures of same

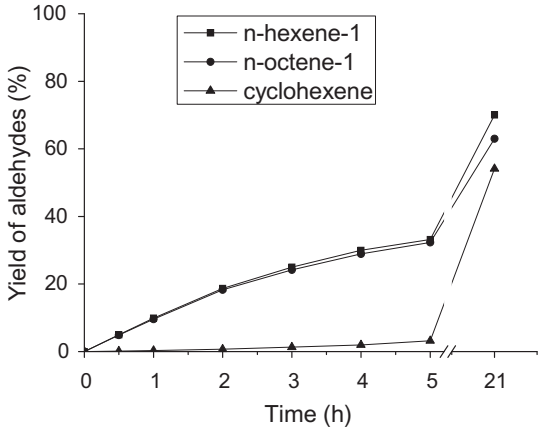

Fig. 10. Yield of aldehydes in hydroformylation of the mixture of *n*-hexene-1, *n*-octene-1, and cyclohexene catalyzed by Rh/MOF-5 (A) at $T = 100$ °C, $P = 50$ bars.

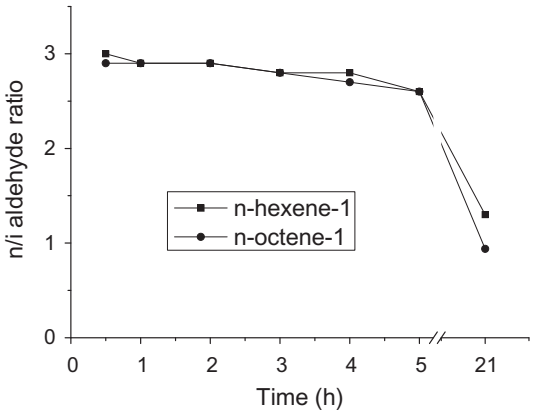

Fig. 11. *n*/*i*-aldehyde ratio in hydroformylation of the mixture of *n*-hexene-1, *n*-octene-1, and cyclohexene in hydroformylation catalyzed by Rh/MOF-5 (A) at $T = 100$ °C, $P = 50$ bars.

Table 2
Catalytic performance of different textural Rh/MOF-5 catalysts in the hydroformylation reaction[a] of *n*-hexene-1.

Reaction time (h)	Rh/MOF-5 (A)		Rh/MOF-5 (B)		Rh/MOF-5 (C)	
	Conversion[b] (%)	Yield[c] (%)	Conversion[b] (%)	Yield[c] (%)	Conversion[b] (%)	Yield[c] (%)
1	30	10	10.7	1.5	76.9	48.4
2	54.2	18.8	40.6	–	86.9	72.2
3	88.5	28.2	70.7	15.6	89.6	77.9
4	98.6	36.8	–	–	–	–
5	98.8	44.5	98.7	33.8	98.9	–
21	99.6	82.2	99.5	76.0	–	–

[a] *Reaction conditions:* $T = 100$ °C, synthesis gas pressure = 50 bars (at 25 °C), 0.1 mol of substrate, 100 mg of catalyst, 30 ml of toluene solvent, 1.000 rpm of stirring.
[b] Total conversion of *n*-olefin to aldehydes and *i*-olefins.
[c] Yield of aldehydes.

composition but different treatment. Besides the Rh/MOF-5 (A) catalyst studied in this paper, a second nano-sized MOF-5 (B) with in tendency more intergrown and slightly smaller particles and a sample consisting of larger well-crystallized crystals MOF-5 (C) were used as catalyst supports. The influence on the catalytic performance is summarized in Table 2 using *n*-hexene-1 as a model molecule.

Interestingly, the catalytic properties of Rh/MOF-5 (C) catalyst consisting of large and well-crystallized crystals differ markedly from nano-sized Rh/MOF-5 catalysts. The olefin is distinctly converted already after short reaction times (1–3 h). The conversions over the large crystal sample are much higher than those over nano-sized one. The conversion of the olefins distinctly proceeds faster already at low reaction time. Additionally, the selectivity to aldehydes is higher, and, correspondingly, the double bond shift reaction is diminished. However, the large crystal Rh/MOF-5 (C) catalyst shows a comparatively low *n*/*i*-aldehyde ratio of ca 0.8–0.9 as usually observed with other inorganic supports.

The catalytic behavior of the second nano-crystalline Rh/MOF-5 (B) catalyst is similar to the nano-sized catalyst (A) mentioned above. However, some differences still exist. The conversions achieved at short reaction times are higher than for nano-sized Rh/MOF-5 (A) catalyst. Again, improved *n*/*i*-aldehyde selectivity is observed. This finding confirms that the high *n*/*i*-aldehyde selectivity is related to nano-sized material.

The lower conversions observed with nano-sized catalysts at short reaction times could indicate that the access of olefins to the pore system, and hence catalytic active species, is lower with nano-sized Rh/MOF-5 (A) and Rh/MOF-5 (B) samples compared to the larger crystal Rh/MOF-5 (C) catalyst. Undertaken nitrogen adsorption measurements nano-sized crystals (A) and (B) showed only slow up take of nitrogen at applied pressure steps indicated by the time required to achieve the adsorption equilibrium again. This indicates diffusion hindrance, e.g. by lattice defects, catenation or intergrowths.

These differences could explain the improved *n*/*i*-aldehyde ratios found with nano-sized samples. In case of well crystallized material the olefins can easily enter the pore system of the MOF-5. In contrast, in case of nano-sized materials mass transfer of olefins into and in the crystals is diminished. Therefore, also diffusion of branched *i*-aldehydes out of the catalyst should be decreased. The catalytic reaction occurs nearby the surface. Both effects could contribute and explain the enhanced selectivity *n*-aldehydes with nano-sized catalysts. This also explains the increased double bond isomerization and lower aldehyde selectivity observed with nano-sized Rh/MOF-5 catalysts. Small differences between nano-sized materials may have a certain impact on the catalytic behavior as found in this study.

4. Conclusion

The investigations show that the metal–organic framework MOF-5 is a suitable catalyst support at least for reactions occurring in organic solvent at relatively low temperature like the hydroformylation of olefins. Furthermore, it could be shown that the textural properties of the support have an important impact on the catalytic properties. Especially, nano-sized Rh/MOF-5 supported catalysts show markedly enhanced *n*-aldehyde selectivity. The *n*/*i*-aldehyde ratios reaching values of up to 3 compared to usually observed values of 0.7–1 for supported catalysts without adding of ligands. This behavior makes MOFs special compared to

common porous materials. Also rhodium MOF structures [43–45] could be of interest, e.g. for hydrogenation as reported [46].

Acknowledgement

This work was in part supported by the German Academic Exchange Service (DAAD), the International Bureau of the Federal Ministry of Education and Research (BMBF, Germany) and granted by the Ministry of Education and Training (MOET, Vietnam) which is gratefully acknowledged by the authors.

References

[1] N.L. Rosi, J. Eckert, M. Eddaoudi, D.T. Vodak, J. Kim, M. O'Keeffe, O.M. Yaghi, Science 300 (2003) 1127–1129.
[2] J.R. Kuppler, D.J. Timmons, Q.-R. Fang, J.-R. Li, T.A. Makal, M.D. Young, D. Yuan, D. Zhao, W. Zhuang, H.-C. Zhou, Coord. Chem. Rev. 253 (2009) 3042–3066.
[3] M. Sabo, A. Henschel, H. Froede, E. Klemm, S. Kaskel, J. Mat. Chem. 17 (2007) 3827–3832.
[4] L. Alaerts, M. Maes, M.A. Van Der Veen, P.A. Jacobs, D.E. De Vos, Phys. Chem. Chem. Phys. 11 (2009) 2903–2911.
[5] F.X.L. i Xamena, A. Abad, A. Corma, H. Garcia, J. Catal. 250 (2007) 294–298.
[6] T.K. Trung, N.A. Ramsahye, P. Trens, N. Tanchoux, C. Serre, F. Fajula, G. Férey, Micropor. Mesopor. Mater. 134 (2010) 134–140.
[7] Z. Ma, B. Moulton, Coord. Chem. Rev. 255 (2011) 1623–1641.
[8] G. Férey, C. Mellot-Draznieks, C. Serre, F. Millange, J. Dutour, S. Surble, I. Margiolaki, Science 309 (2005) 2040–2042.
[9] K. Schlichte, T. Kratzke, S. Kaskel, Micropor. Mesopor. Mater. 73 (2004) 81–88.
[10] W. Böhlmann, A. Pöppl, M. Sabo, S. Kaskel, J. Phys. Chem. B 110 (2006) 20177–20181.
[11] M. Dogru, A. Sonnauer, A. Gavryushin, P. Knochel, T. Bein, Chem. Commun. 47 (2011) 1707–1709.
[12] S. Hermes, M.-K. Schröter, R. Schmid, L. Khodeir, M. Muhler, A. Tissler, R.W. Fischer, R.A. Fischer, Angew. Chem. Int. Ed. 44 (2005) 6237–6241.
[13] A. Schaate, M. Schulte, M. Wiebcke, A. Godt, P. Behrens, Inorg. Chim. Acta 362 (2009) 3600–3606.
[14] N.B. Pathan, A.M. Rahatgaonkar, M.S. Chorghade, Catal. Commun. 12 (2011) 1170–1176.
[15] D. Xuan-Dong, H. Vinh-Thang, S. Kaliaguine, Micropor. Mesopor. Mater. 141 (2011) 135–139.
[16] M. Marchetti, S. Paganelli, E. Viel, J. Mol. Catal. A 222 (2004) 143–151.
[17] M. Bortenschlager, J. Schütz, D.V. Preysing, O. Nuyken, W.A. Herrmann, R. Weberskirch, J. Organomet. Chem. 690 (2005) 6233–6237.
[18] P.C.J. Kamer, J.N.H. Reek, P.W.N.M. van Leeuwen, Non addicted nature, in: B. Heaton (Ed.), Mechanisms in Homogeneous Catalysis, A spectroscopic Approach, Wiley–VCH, Weinheim, 2005, p. 231.
[19] H.H. Storch, Adv. Catal. 1 (1948) 115.
[20] H.H. Storch, N. Golumbic, R.B. Anderson, The Fishcher–Tropsch and Related Syntheses, Wiley–VCH, 1951. p. 441.
[21] C.D. Frohning, C.W. Kohlpaintner, H.-W. Bohnen, Applied Homogeneous Catalytic with Organometallic Compounds – A Comprehensive Handbook in Three Volumes, second ed., Wiley–VCH, 2002.
[22] S.K. Sharma, P.A. Parikh, R.V. Jasra, J. Mol. Catal. 316 (2010) 153–162.
[23] C.D. Frohning, C.W. Kohlpaintner, Appl. Homog. Catal. Organomet. Compd. (2003) 31–33.
[24] H.-W. Bohnen, B. Cornils, Adv. Catal. 47 (2002) 1–64.
[25] M.S. Shaharun, B.K. Dutta, H. Mukhtar, S. Maitra, Chem. Eng. Sci. 65 (2010) 273–281.
[26] J. A Bae, K.-C. Song, J.-K. Jeon, Y.S. Ko, Y.-K. Park, J.-H. Yim, Micropor. Mesopor. Mater. 123 (2009) 289–295.
[27] K. Mukhopadhyay, R.V. Chaudhari, J. Catal. 213 (2003) 73–77.
[28] D. Han, X. Li, H. Zhang, Z. Liu, J. Li, C. Li, J. Catal. 243 (2006) 318–328.
[29] L. Huang, S. Kawi, Catal. Lett. 92 (2004) 57–62.
[30] T.A. Kainulainen, M.K. Niemelä, A.O.I. Krause, J. Mol. Catal. A 122 (1997) 39–49.
[31] L. Huang, Y. He, S. Kawi, J. Mol. Catal. 213 (2004) 241–249.
[32] U. Mueller, M. Schubert, F. Teich, H. Puetter, K. Schierle-Arndt, J. Pastré, J. Mater. Chem. 16 (2006) 626–636.
[33] S. Hermes, F. Schröder, S. Amirjalayer, R. Schmid, R.A. Fischer, J. Mater. Chem. 16 (2006) 2464–2472.
[34] L. Huang, H. Wang, J. Chen, Z. Wang, J. Sun, D. Zhao, Y. Yan, Micropor. Mesopor. Mater. 58 (2003) 105–114.
[35] S.S. Kaye, A. Dailly, O.M. Yaghi, J.R. Long, J. Am. Chem. Soc. 129 (2007) 14176–14177.
[36] H. Li, M. Eddaoudi, M. O'Keeffe, O.M. Yaghi, Nature 402 (1999) 276–279.
[37] D. Saha, S. Deng, J. Colloid Interface Sci. 348 (2010) 615–620.
[38] J. Li, S. Cheng, Q. Zhao, P. Long, J. Dong, Int. J. Hydrog. Energy 34 (2009) 1377–1382.
[39] S. Gao, N. Zhao, M. Shu, S. Che, Appl. Catal. 388 (2010) 196–201.
[40] F. Schröder, D. Esken, M. Cokoja, M.W.E. van den Berg, O.I. Lebedev, G.V. Tendeloo, B. Walaszek, G. Buntkowsky, H.-H. Limbach, B. Chaudret, R.A. Fischer, J. Am. Chem. Soc. 130 (2008) 6119–6130.
[41] R.S. Mikhail, E. Robens, Microstructure and Thermal Analysis of Solid Surfaces, John Wiley and Sons, 1983.
[42] H. Kosslick, R. Bräunig, R. Eckelt, J. Harloff, S. Mothes, H. Häring, S. Wilhelm, A. Schulz, J. Chem. Chem. Eng. 5 (2011) 170–176.
[43] T. Ueda, K. Kurokawa, T. Eguchi, C. Kachi-Terajima, S. Takamizawa, J. Phys. Chem. C 111 (2007) 1524–1534.
[44] S. Takamizawa, E.-I. Nakata, T. Saito, Cryst. Eng. Comm. 6 (2004) 39–41.
[45] D.L. Reger, A. Debreczeni, M.D. Smith, Inorg. Chim. Acta 378 (2011) 42–48.
[46] S. Naito, T. Tanibe, E. Saito, T. Miyao, W. Mori, Chem. Lett. 30 (2001) 1178.